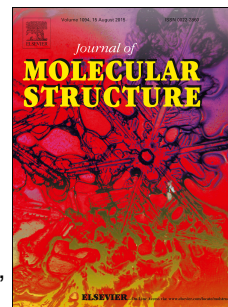


# Accepted Manuscript

Synthesis, single crystal structure, spectroscopic characterization and molecular properties of (2E)-3-(2,6-dichlorophenyl)-1-(3,4-dimethoxyphenyl)prop-2-en-1-one

C.S. Chidan Kumar, C.K. Quah, V. Balachandran, H.K. Fun, A.M. Asiri, S. Chandraju, M. Karabacak



PII: S0022-2860(16)30183-1

DOI: [10.1016/j.molstruc.2016.02.089](https://doi.org/10.1016/j.molstruc.2016.02.089)

Reference: MOLSTR 22298

To appear in: *Journal of Molecular Structure*

Received Date: 9 November 2015

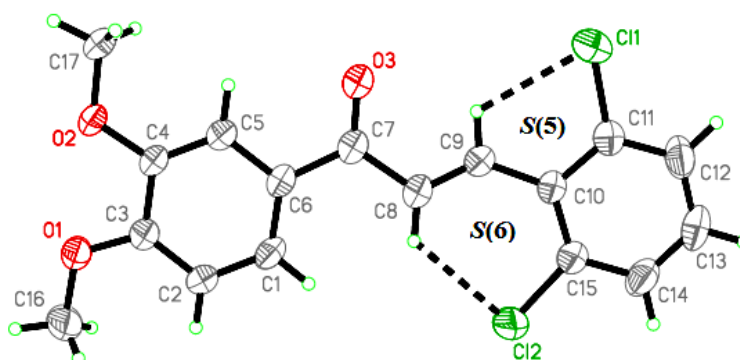
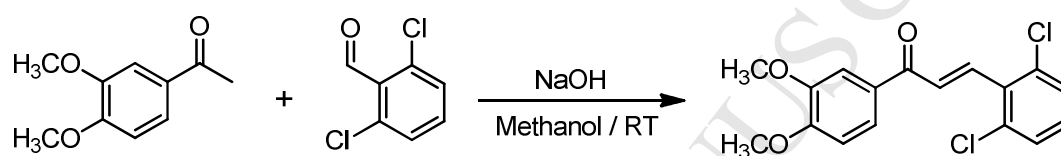
Revised Date: 24 February 2016

Accepted Date: 24 February 2016

Please cite this article as: C.S. Chidan Kumar, C.K. Quah, V. Balachandran, H.K. Fun, A.M. Asiri, S. Chandraju, M. Karabacak, Synthesis, single crystal structure, spectroscopic characterization and molecular properties of (2E)-3-(2,6-dichlorophenyl)-1-(3,4-dimethoxyphenyl)prop-2-en-1-one, *Journal of Molecular Structure* (2016), doi: [10.1016/j.molstruc.2016.02.089](https://doi.org/10.1016/j.molstruc.2016.02.089).

This is a PDF file of an unedited manuscript that has been accepted for publication. As a service to our customers we are providing this early version of the manuscript. The manuscript will undergo copyediting, typesetting, and review of the resulting proof before it is published in its final form. Please note that during the production process errors may be discovered which could affect the content, and all legal disclaimers that apply to the journal pertain.

## Graphical abstract



**Synthesis, single crystal structure, spectroscopic characterization and molecular properties of (2E)-3-(2,6-dichlorophenyl)-1-(3,4-dimethoxyphenyl)prop-2-en-1-one**

C.S. Chidan Kumar<sup>1,2</sup>, C.K. Quah<sup>1</sup>, V. Balachandran<sup>3</sup>, H.K. Fun<sup>1,4#</sup>, A.M. Asiri<sup>5,6</sup>, S. Chandraju<sup>7</sup>, M. Karabacak<sup>8,\*</sup>

<sup>1</sup> X-ray Crystallography Unit, School of Physics, Universiti Sains Malaysia, USM, Penang, Malaysia

<sup>2</sup> Department of Engineering Chemistry, Alva's Institute of Engineering & Technology, Mijar, Moodbidri, Mangalore (D.K), Karnataka, India

<sup>3</sup> Centre for Research, Department of Physics, AA Government Arts College, Musiri, India

<sup>4</sup> Department of Pharmaceutical Chemistry, College of Pharmacy, King Saud University, Riyadh, Saudi Arabia

<sup>5</sup> Department of Chemistry, Faculty of Science, King Abdulaziz University, Jeddah, Saudi Arabia

<sup>6</sup> Center of Excellence for Advanced Materials Research, King Abdulaziz University, Jeddah, Saudi Arabia

<sup>7</sup> Department of Sugar Technology and Chemistry, Sir M. Visvesvaraya PG Center, University of Mysore, Tubinakere, Karnataka, India

<sup>8</sup> Department of Mechatronics Engineering, H.F.T. Technology Faculty, Celal Bayar University, Turgutlu, Manisa, Turkey

---

\* Corresponding author: [mehmet.karabacak@cbu.edu.tr](mailto:mehmet.karabacak@cbu.edu.tr)

Tel.: +90 236 314 10 10, Fax: +90 236 314 20 20

# Additional correspondence author: [hkfun@usm.my](mailto:hkfun@usm.my) ; [hfun.c@ksu.edu.sa](mailto:hfun.c@ksu.edu.sa)

Tel.: +91 9894253672; Fax: +91 4326 262630.

## Abstract

A novel (2E)-3-(2,6-dichlorophenyl)-1-(3,4-dimethoxyphenyl)prop-2-en-1-one (DCPDMP) compound has been synthesized and its single crystal has been grown by slow evaporation technique. The structure of the compound has been characterized by FT-IR, FT-Raman and single-crystal X-ray diffraction techniques. The optimized molecular structure, vibrational wavenumbers, corresponding vibrational assignments of the compound have been investigated by means of the density functional theory. The molecule crystallizes in triclinic system, space group P-1 with  $a = 7.6179$  (7),  $b = 8.5023$  (7),  $c = 12.1967$  (10) Å,  $V = 764.39$  (11) Å<sup>3</sup> and two molecules in the unit cell. The crystal structure is primarily stabilized through intramolecular C–H...Cl and C–H...O hydrogen bonds and intermolecular C–H...O and weak C–H... $\pi$  interactions. These inter- and intramolecular interactions are analyzed. Moreover, the molecular electrostatic potential surface of the molecule has been constructed. Global and local reactivity descriptors and dipole moment ( $\mu$ ), static polarizability ( $\alpha$ ), first order hyperpolarizability ( $\beta$ ) and optical gap ( $\Delta E$ ) have been also calculated to study the nonlinear optical (NLO) property of the title compound.

**Keywords:** Crystal growth; FT-IR and FT-Raman spectra; DFT; NBO and NLO; HOMO-LUMO.

## 1. Introduction

The design and synthesis of organic molecules exhibiting nonlinear optical (NLO) properties have been motivated by their potential for applications in optical communications, optical computing, data storage, frequency mixing, and optical switching [1]. Chalcones are interesting organic NLO materials with good crystallizability, high second harmonic generation (SHG) efficiency compared to urea, and optical transparency extending down to the blue region [2,3]. It has been generally understood that the second-order molecular nonlinearity in chalcones can be enhanced by large delocalized  $\pi$ -electron systems with strong donor and acceptor groups. The basic strategy of using electron-donor and electron-acceptor substituents to polarize the  $\pi$ -electron system of organic materials has been illustrious for developing the NLO chromophores possessing large molecular nonlinearity. Many researchers suggested that the theoretical hyperpolarizability studies on these molecules that

the carbonyl group present at the middle in these molecules splits the conjugated system into relatively two independent parts and the electron donors, such as  $-\text{OCH}_3$ ,  $-\text{CH}_3$ ,  $-\text{Cl}$  and  $-\text{Br}$ , are the best donor groups for enhancing SHG in chalcones [4,-6].

To the best of our knowledge, this compound has not been reported and studied as far as its relevance is concerned. The aim of this paper is to describe the synthesis, molecular structure and single-crystal growth of DCPDMP. The structure of the compound was characterized by FT-IR and FT-Raman and confirmed by single crystal X-ray diffraction techniques. Vibrational frequencies and geometric parameters of DCPDMP in the ground state were calculated by using B3LYP/6-31G(d) and 6-31G(d,p) basis sets. A detailed quantum chemical study will aid in making definite assignments to fundamental normal modes of DCPDMP and in clarifying the experimental data for this important molecule. In addition, Density Functional Theory (DFT) method in conjunction with the BLYP functional using 6-31G(d) and 6-31G(d,p) basis sets was employed to predict the dipole moments, polarizability, hyperpolarizability, frontier orbital energy, molecular electrostatic potential surface, natural bond orbital and reactivity descriptors with molecular geometry. The findings of these spectroscopic and theoretical studies are herein reported.

## 2. Experimental methods

### 2.1. Synthesis

The reagents and solvents for the synthesis were obtained from Aldrich Chemical Co., and were used without additional purification. New chalcones were designed and synthesized by the reaction of 1-(3,4-Dimethoxyphenyl) ethanone with substituted 2,6-dichlorobenzaldehyde in presence of catalytic amount of NaOH in methanol, as shown in **Scheme 1**. 1-(3,4-Dimethoxyphenyl) ethanone (0.01 mol) and 2,6-dichlorobenzaldehyde (0.01 mol) were dissolved in 20 ml methanol. A catalytic amount of NaOH was added to the solution drop-wise with vigorous stirring. The reaction mixture was stirred for about 5-6 hours at room temperature. The progress of the reaction was monitored by TLC. The formed crude products were filtered, washed successively with distilled water and recrystallized from ethanol to get the title chalcone. Crystals suitable for X-ray diffraction studies were obtained from acetone solution by slow evaporation technique at room temperature. Melting point (384–386 K) was determined by Stuart Scientific (UK) apparatus. The purity of the compound was confirmed by thin layer chromatography using Merck silica gel 60 F254 coated aluminum plates.

## 2.2. Instrumentation

The compound DCPDMP on powder form was synthesized and it is used to record the FT-IR and FT-Raman spectra. The FT-IR spectrum for the compound was recorded on a UV–VIS–NIR Perkin Elmer Lambda 900 spectrometer in the range of 4000–400  $\text{cm}^{-1}$  without using NaCl plates or KBr pellets (in solid form). The FT-Raman spectrum was recorded using the 1064 nm line of a Nd:YAG laser as the excitation wavelength in the region 3500–100  $\text{cm}^{-1}$  on a Nexus 670 spectrophotometer.

## 2.3. Computational methods

Thorough information including structural attributes and vibrational modes of DCPDMP has been presented in a comparative way using (DFT) strategy with different basis sets. All the calculations were performed using Gaussian 09 program suite [7]. Geometry optimization was carried out at DFT method by using 6-31G (d) and 6-31G (d,p) basis sets to portray all stationary points as minima. Then, these optimized structural parameters were used for frequency calculations ensuing IR and Raman frequencies. To obtain better agreement with the experimental and theoretical results standard scale factors (correction factors) were used. At B3LYP method with both the basis sets like 6-31G(d)/6-31G(d,p) a scaling factor of 0.98 has been recommended for all frequencies  $<1800 \text{ cm}^{-1}$ . A scaling factor of 0.96 was utilized for C–H stretching modes due to large anharmonicities in higher wavenumber region  $>2700 \text{ cm}^{-1}$ . However, for vibrational modes observed in lower wavenumber region  $<1500 \text{ cm}^{-1}$  a scaling factor 1.0 has been prescribed. Correction factors for B3LYP is therefore much more useful in bringing the experimental and theoretical results closer to each other. The vibrational modes are assigned on the basis of Total Energy Distribution (TED) analysis using Vibrational Energy Distribution Analysis (VEDA) program [8]. The Natural Bond Orbital (NBO) calculations [9] were performed by using NBO 5.0 Program as implemented in the Gaussian 09W [7] package at B3LYP/6-31G(d,p) method in order to understand various second order interactions between the filled orbital of one subsystem and vacant orbital of another subsystem, which are the measure of the intramolecular delocalization or hyper conjugation. The highest occupied and lowest unoccupied molecular orbitals (HOMO and LUMO) of the compound were analyzed.

## 3. Results and Discussion

The geometrical parameters of the synthesized compound are reported and discussed

with respect to the X-ray data. This is followed by discussion of the experimental and theoretical vibrational frequencies and their intensities. The frontier molecular orbitals, natural bond orbital (NBO) are also explored. Furthermore, in order to show nonlinear optics activity of the molecule, the dipole moment, linear polarizability and first order hyperpolarizability are analyzed.

### 3.1. X-ray crystallographic studies

Yellow, block shaped single crystal of DCPDMP, with dimensions of 0.48 mm × 0.20 mm × 0.21 mm was selected and mounted on a BRUKER APEX-II CCD diffractometer with a fine-focus sealed tube graphite-monochromated Mo K $\alpha$  radiation ( $\lambda = 0.71073 \text{ \AA}$ ) at 294 K in the range of  $1.7 \leq \theta \leq 26.0^\circ$ . The data were processed with SAINT and corrected for absorption using SADABS [10]. A total of 12215 reflections were collected, of which 2986 were independent and 2459 reflections with  $I > 2\sigma(I)$ . The structures were solved by direct method using the program SHELXTL [11] and were refined by full-matrix least squares technique on  $F^2$  using anisotropic displacement parameters for all non-hydrogen atoms. All the hydrogen atoms were positioned geometrically [C—H = 0.93–0.96  $\text{\AA}$ ] and refined using riding model with isotropic displacement parameters set to 1.2 or 1.5 (methyl group) times the equivalent isotropic U values of the parent carbon atoms. A rotating group model was used for methyl groups. The final full-matrix least squares refinement gave  $R = 0.043$  and  $wR = 0.135$  ( $w = 1/[\sigma^2(F_o^2) + (0.0678 P)^2 + 0.2837P]$  where  $P = (F_o^2 + 2F_c^2)/3$ ,  $S = 1.09$ ,  $(\Delta/\sigma)_{\text{max}} = 0.001$ ,  $\Delta\rho_{\text{max}} = 0.28 \text{ e \AA}^{-3}$  and  $\Delta\rho_{\text{min}} = -0.23 \text{ e \AA}^{-3}$ . A summary of crystal data and parameters for structure refinement details are given in **Table 1**.

The molecular structure of the title compound, C<sub>17</sub>H<sub>14</sub>Cl<sub>2</sub>O<sub>3</sub>, with atom labelling scheme drawn at 50% probability displacement ellipsoid is depicted in **Fig. 1**. The interplanar angle between the dimethoxyphenyl and 2, 6-dichlorophenyl rings is  $0.90 (11)^\circ$ . Both of these phenyl rings are connected via central prop-2-en-1-one bridge. The molecule exist in trans configuration with respect to the C8=C9 double bond of the central enone group, which is confirmed by the C7—C8=C9—C10 torsion angle of  $176.1 (3)^\circ$ . In the structure, two weak intramolecular C9—H9A $\cdots$ C11 and C8—H8A $\cdots$ C12 interactions (**Table 2, Fig. 1**) generate S (5) and S (6) ring motif's respectively [12]. These interactions contributed to the planarity of the molecule. The methoxy group attached to C4 atom is close to planar with the C17—O2—C4—C5 torsion angle of  $0.2 (3)^\circ$  and another methoxy group attached to C3 atom is slightly twisted with the C16—O1—C3—C2 torsion angle of  $-7.9 (4)^\circ$ . Besides Cl atoms are planar

to the ring. In the crystal structure, intermolecular C—H...O hydrogen bonds (**Table 2**) link the molecule into chains in head-to-tail fashion. Further, the adjacent molecule of these chains are connected via Cl...Cl (3.494 Å) short contacts producing one-dimensional sheets extending along b axis direction. These molecular sheets are stacked into layers (**Figs. 2 and 3**) along *ac* plane by  $\pi$ — $\pi$  interactions with Cg1...Cg1 and Cg2...Cg2 distance of 3.7123 (13) and 3.5843 (14) respectively (where, Cg1 is the centroid of the C1—C6 benzene ring and Cg2 is the centroid of the C10—C15 benzene ring). In addition, crystal structure features for a weak C—H... $\pi$  interaction (**Table 2**) involving the centroid of the C1—C6 benzene ring. The bond length and bond angles agree with the literature values and are comparable with those reported earlier [13-15].

The optimized parameters (bond lengths, bond angles, and dihedral angles) of the title compound [**Fig. 4**] have been obtained using the B3LYP/6-31G(d) and 6-31G(d,p) method. Some selected geometrical parameters experimentally obtained and theoretically calculated are listed in **Table 3**. For example, the double C16 = O17 and C11 = C14 double bond lengths were calculated as 1.23 and 1.34 Å, respectively, which are in a good agreement with experimental values (1.21 and 1.30 Å). Most of the bond lengths and bond angles are slightly deviating when comparing with the experimental data for both DFT functional. These differences are probably due to the theoretical calculations belong to isolated molecule in gaseous phase while the experimental results belongs to molecule in solid state.

### 3.2. Vibrational spectral analysis

The observed and calculated vibrational frequencies along with assignments have been summarized in **Table 4**. For visual comparison, the observed and calculated (simulated) infrared and Raman spectra of the title compound were presented in **Figs. 5 and 6**, which is convenient to discuss the vibrational spectra of the title molecule as described below:

#### C—Cl vibrations

The vibration belonging to the bond between the ring and halogen atoms is worth to discuss here, since mixing of the vibrations is possible due to the lowering of the molecular symmetry and the presence of heavy atom on the periphery of the molecule [16]. Generally, stretching and bending vibrations of C—Cl bonds lie in the low wavenumber region of the spectrum [17,18]. Compounds with more than one chlorine atom exhibit very strong bands

due to the asymmetric and symmetric stretching modes. The vibrations of C–X group (X; F, Cl, Br) in the frequency range give generally strong bands in the region 1292–485 $\text{cm}^{-1}$  [19,20]. Based on the above literature values the strong band is observed at 767  $\text{cm}^{-1}$  in FT-IR. The theoretically calculated values of C–Cl stretching vibrations are found to be 771 and 764  $\text{cm}^{-1}$  by B3LYP/6-31G(d) and B3LYP/6-31G(d,p), respectively. The C–Cl in-plane bending modes have strong to medium intensity generally in the region 550–250  $\text{cm}^{-1}$ . In the present study, C–Cl in plane bending and out-plane-bending vibrations are found and the TED values are shown in **Table 4**.

### Carbonyl and ethylenic bridge vibrations

The carbonyl bands are most characteristic bands of infrared and Raman spectra [21–23]. The carbonyl vibration bands in ketones normally having a strong intensity are expected in the region 1715–1680  $\text{cm}^{-1}$  [23]. The carbon–oxygen double bond is formed by  $P\pi -P\pi$  between carbon and oxygen atoms and the lone pair of electron on oxygen also determines the nature of carbonyl group. The C=O stretching vibration band can be easily identified from the IR and Raman spectra, and because of the degree of conjugation the strength and polarizations are increasing. The C16=O17 stretching is observed in FT-Raman as a strong band at 1661  $\text{cm}^{-1}$ , which is confirmed by the TED values. The deviation from the calculated wavenumber for this mode can be attributed to the under estimation of  $\pi$ -electron delocalisation due to conjugation and hydrogen bonding network inside the crystal. In DCPDMP, the C=C stretching vibrations of ethylenic bridge overlaps with vibrations of C16=O17 stretching mode. The intense band at 1650  $\text{cm}^{-1}$  in IR spectrum has been assigned to C11=C14 stretching mode which is coupled with C16=O17 stretching.

### C–H vibrations

Normally, the aromatic ring C–H stretching vibrations occurs in the region 3100–3000  $\text{cm}^{-1}$  [16,24–27]. In this region, the bands are not affected appreciably by the nature of the substituent. For the C–H stretching vibrations, we have observed the FT-IR bands at 3109, 3078, 3005  $\text{cm}^{-1}$  and 3113 and 3081  $\text{cm}^{-1}$  in FT-Raman spectrum. These modes are stretching modes as evident from the TED column shown in **Table 4**. The calculated values of these modes are good agreement with maximum contribution of TED. The C–H in plane bending vibrations usually occur in the region 1400–1050  $\text{cm}^{-1}$  and the C–H out of plane bending vibrations observe in the range of 1000–675  $\text{cm}^{-1}$  [25,28]. In our study, the C–H in plane

bending vibrations have been observed at 1418, 1309, 1253 and 1183  $\text{cm}^{-1}$  in FT-IR and 1419, 1161 and 1096  $\text{cm}^{-1}$  in FT-Raman and their corresponding theoretical values are quite compatible. Also the C–H out of plane vibrations have been observed at 978 and 841  $\text{cm}^{-1}$  in FT-IR and 774  $\text{cm}^{-1}$  in FT-Raman. These vibrations also show good agreement with theoretically scaled harmonic wavenumber values.

### C–C vibrations

The C–C ring stretching vibrations are expected within the region 1650–1200  $\text{cm}^{-1}$ . In general, the bands of variable intensity are observed at 1625–1590, 1575–1590, 1470–1540, 1430–1465 and 1280–1380  $\text{cm}^{-1}$  from the frequency ranges given by Varsanyi [25] for the five bands in the region. The frequency bands at 1650, 1591, 1575, 1350 and 1305  $\text{cm}^{-1}$  in FT-IR and at 1613, 1581 and 1565  $\text{cm}^{-1}$  in FT-Raman were assigned to the C–C stretching vibrations for our molecule. The theoretical computed C–C–C in plane and out of plane bending vibrations by the B3LYP/6-31G(d,p) shows good agreement with the recorded spectral data. The other wavenumbers of the ring groups such as; torsional and rocking modes are also assigned, and presented in **Table 4**. All these calculated values are in good agreement with the experimental data.

### Methoxy group vibrations

The methoxy group has two C–H stretching vibrations: symmetric and asymmetric stretching. The asymmetric stretch is usually at higher wavenumber than the symmetric stretch. The methoxy C–H symmetric stretching modes usually appear in the region 2825–2870  $\text{cm}^{-1}$  where as asymmetric mode lie in the range of 2925–2985  $\text{cm}^{-1}$  [22,24,29]. The FT-IR band at 2937 and 2841  $\text{cm}^{-1}$  and the corresponding FT-Raman band at 2936 and 2839  $\text{cm}^{-1}$  are assigned to  $\text{CH}_3$  symmetric stretching vibration. The FT-IR band at 3000 and 2962  $\text{cm}^{-1}$  are assigned to  $\text{CH}_3$  asymmetric stretching modes. The asymmetric and symmetric bending vibrations of methyl group are expected in the region 1465–1440  $\text{cm}^{-1}$  and 1390–1370  $\text{cm}^{-1}$ , respectively [22,24]. The contribution of intermolecular interactions on methoxy stretching modes is confirmed by the better coincidence of band position in the solution spectrum with the computed vibrational wavenumbers. The methyl asymmetric bending appears as a strong band in FT-IR at 1458  $\text{cm}^{-1}$ . The methyl frequencies are to some extent sensitive to the electronegativity of the attached atom and the symmetric deformation is particularly sensitive and it appears at 1435 in FT-IR and 1436  $\text{cm}^{-1}$  in FT-Raman. The strong band in FT-IR at

1151  $\text{cm}^{-1}$  and 1177  $\text{cm}^{-1}$  in FT-Raman are assigned to  $\text{CH}_3$  in plane rocking mode. The  $\text{CH}_3$  out of plane rocking mode are appeared with mixed modes which are found by TED values shown in **Table 4**. The C=O stretching vibration of the compound is observed at 1661 and 1650  $\text{cm}^{-1}$  in FT-Raman and FT-IR spectra and calculated at 1660 and 1650  $\text{cm}^{-1}$  coupled with CC stretching mode. The torsion mode of the O- $\text{CH}_3$  group was observed at 228 and 148  $\text{cm}^{-1}$  in FT-Raman.

The remainder of the observed and calculated wavenumbers and their assignments of the compound are shown in **Table 4**.

### 3.3. Frontier molecular orbitals (FMOs)

The frontier molecular orbital determine the way in which the molecule interacts with other species. HOMO (highest occupied molecular orbital), which can be thought the outermost orbital containing electrons, tends to give these electrons such as an electron donor. On the other hand, LUMO (lowest unoccupied molecular orbital) can be thought the innermost orbital containing free places to accept electrons [30]. Therefore, while the energy of the HOMO is directly related to the ionization potential, LUMO energy is directly related to the electron affinity. Energy difference between HOMO and LUMO orbital is called as energy gap that is an important stability for structures [31]. HOMO-LUMO helps to characterize the chemical reactivity and kinetic stability of the molecule [32]. A molecule with a small gap is more polarized and is known as soft molecule. Recently, the energy gap between HOMO and LUMO has been used to prove the bioactivity from intramolecular charge transfer (ICT) [33,34] because it is a measure of electron conductivity. The frontier orbital (HOMO, LUMO) of DCPDMP, with B3LYP/6-31G(d,p) method are plotted in **Fig. 7**. The HOMO and LUMO energy gap of DCPDMP calculated by B3LYP/6-31G(d) and 631G(d,p) methods are given in **Table 5**. According to B3LYP/6-31G(d,p) calculation, the energy band gap ( $\Delta E$ ) (translation from HOMO to LUMO) of the molecule is about 6.0162 eV. The highest occupied molecular orbital is localized mainly on both the rings, while LUMO is localized carbonyl, methoxy, ethylenic bridge groups and benzene ring.

### 3.4. Global and local reactivity descriptors

Quantum chemical methods have been proven a very useful tool to study chemical systems stabilized by hydrogen bonds. By using HOMO and LUMO energy values for a

molecule, the global chemical reactivity descriptors of molecules such as hardness, chemical potential, softness, electronegativity and electrophilicity index as well as local reactivity have been defined [35-37]. Pauling introduced the concept of electronegativity as the power of an atom in a molecule to attract electrons to it. Hardness ( $\eta$ ), chemical potential ( $\mu$ ) and electronegativity ( $\chi$ ) and softness are defined follows.

$$\mu = \left(\frac{\partial E}{\partial N}\right)_{v(r)}$$

$$\eta = 1/2\left(\frac{\partial^2 E}{\partial N^2}\right)_{v(r)}$$

Operational schemes for the calculation of chemical hardness are based on a finite difference method and thus:

$$\mu \approx 1/2(E_{HOMO} + E_{LUMO})$$

$$\eta \approx -1/2(I.P + E.A)$$

where I.P = Ionization Potential and E.A = Electron Affinity.

These global quantities, as well as the mean polarizability values ( $\alpha$ ), have been found very useful and complementary tools for the description of chemical reactivity in connection with minimum polarizability and maximum hardness principles. Considering the chemical hardness, large HOMO–LUMO gap means a hard molecule and small HOMO–LUMO gap means a soft molecule. One can also relate the stability of the molecule to hardness, which means that the molecule with least HOMO–LUMO gap means, it is more reactive.

Recently Parr et al. [37] have defined a new descriptor to quantify the global electrophilic power of the molecule as electrophilicity index ( $\omega$ ), which defines a quantitative classification of the global electrophilic nature of a molecule. The defined electrophilicity index ( $\omega$ ) as follows:

$$\omega = \frac{\mu^2}{2}$$

Using the above equations, the chemical potential, hardness and electrophilicity index have been calculated for DCPDMP and their values are shown in **Table 5**. The calculated values of the hardness, electronegativity, chemical potential, and electrophilicity index of our molecule in gas phase is 1.9243, 4.0919, -4.0919 and 4.3506, respectively.

### 3.5. Natural Bond Orbital analysis

NBO analysis provides the most accurate possible ‘natural Lewis structure’ picture of  $\phi$ , because all the orbital details are mathematically chosen to include the highest possible percentage of the electron density. A useful aspect of the NBO method is that it gives information about interactions in both filled and virtual orbital spaces that could enhance the analysis of intra- and inter-molecular interactions. The second-order Fock matrix was carried out to evaluate the donor–acceptor interactions in NBO analysis [38,39]. The interactions result is the loss of occupancy from the localized NBO of the idealized Lewis structure into an empty non-Lewis orbital. For each donor ( $i$ ) and acceptor ( $j$ ), the stabilization energy  $E(2)$  associated with the delocalization  $i \rightarrow j$  is estimated as

$$E(2) = \Delta E_{ij} = q_i \frac{F(i, j)^2}{\epsilon_j - \epsilon_i}$$

where  $q_i$  is the donor orbital occupancy,  $\epsilon_i$  and  $\epsilon_j$  are diagonal elements and  $F(i, j)$  is the off diagonal NBO Fock matrix element. Some electron donor orbital, acceptor orbital and the interacting stabilization energy resulting from the second-order micro-disturbance theory are reported [40,41]. The larger the  $E(2)$  value, the more intensive is the interaction between electron donors and electron acceptors, i.e., the more donating tendency from electron donors to electron acceptors and the greater the extent of conjugation of the whole system. Delocalization of electron density between occupied Lewis-type (bond or lone pair) NBO orbital and formally unoccupied (anti-bond or Rydberg) non-Lewis NBO orbital correspond to a stabilizing donor–acceptor interaction. NBO analysis has been performed on the molecule at the B3LYP/6–31G(d,p) level in order to elucidate the intra-molecular, re-hybridization and delocalization of electron density within the molecule.

The strong intramolecular hyperconjugative interaction of the s and p electrons of C–C to the anti C–C bond of the ring leads to stabilization of some part of the ring as evident from **Table 6**. There occurs a strong intramolecular hyperconjugative interaction of the  $\pi(\text{C4–C5})$  orbital with the  $\pi^*(\text{C2–C3})$  orbital which leads to the stabilization of 21.10 kcal/mol. This enhanced  $\pi^*(\text{C2–C3})$  NBO further conjugates with  $\pi^*(\text{C4–C5})$  resulting in an enormous  $E(2)$  energy of 228.76 kcal/mol. The hyperconjugative interaction is maximum between lone pair of LP(2) O31 and antibonding orbital of the  $\pi^*(\text{C22–C23})$ . The intramolecular hyperconjugative interactions result in ICT causing stabilization of the system. These interactions are observed as an increase in ED that weakens the respective bonds.

### 3.6. Nonlinear Optical Features

The computational approach allows the determination of molecular NLO properties as an inexpensive way to design molecules by analyzing their potential before synthesis and to determine high order hyperpolarizability tensors of molecules. The simplest polarizability ( $\alpha$ ), characterizes the ability of an electric field to distort the electronic distribution of a molecule.

The first hyperpolarizability ( $\beta$ ) of this novel molecular system, and the related properties ( $\beta$ ,  $\alpha_0$  and  $\Delta\alpha$ ) were calculated based on the finite-field approach. In the presence of an applied electric field, the energy of a system is a function of the electric field. Polarizability and hyperpolarizability characterize the response of a system in an applied electric field [42]. They determine not only the strength of molecular interactions (long-range interaction, dispersion force, etc.) and the cross sections of different scattering and collision process but also the NLO properties of the system [43,44]. First hyperpolarizability is a third rank tensor that can be described by a 3x3x3 matrix. The 27 components of the 3D matrix can be reduced to 10 components due to the Kleinman symmetry [45], and can be given in the lower tetrahedral format. It is obvious that the lower part of the 3x3x3 matrices is tetrahedral. The components of are defined as the coefficients in the Taylor series, with expansion of the energy in the external electric field. When the external electric field is weak and homogeneous, this expansion becomes:

$$E = E^0 - \mu_\alpha F_\alpha - \frac{1}{2} \alpha_{\alpha\beta} F_\alpha F_\beta - \frac{1}{6} \beta_{\alpha\beta\gamma} F_\alpha F_\beta F_\gamma + \dots$$

where  $E^0$  is the energy of the unperturbed molecules  $F_\alpha$  is the field at the origin,  $\mu_\alpha$ ,  $\alpha_{\alpha\beta}$  and  $\beta_{\alpha\beta\gamma}$  are the components of the dipole moment, polarizability and the first hyperpolarizabilities, respectively.

The total static dipole moment, the mean polarizability, the anisotropy of the polarizability and the mean first-order hyperpolarizability of the title compound has been calculated using B3LYP/6-31G(d) and 6-31G(d,p) levels. The conversion factor  $\alpha$ ,  $\beta$  and HOMO and LUMO energies in atomic and cgs units: 1 atomic unit (a.u.) = 0.1482 x 10<sup>-24</sup> electrostatic unit (esu) for  $\alpha$ ; 1 a.u. = 8.6393 x 10<sup>-33</sup> esu for  $\beta$ ; 1 a.u. = 27.2116 eV (electron volt) for HOMO and LUMO energies.

This title compound has a larger dipole moment (**Table 7**), and that the stronger dipole

moment of DCPDMP leads to increased polarity. The different charge distributions result in completely different orientations of the (calculated) dipole moments. In **Table 7**, the results of the electronic dipole moment polarizabilities ( $\alpha$  and  $\Delta\alpha$ ) and the first hyperpolarizability ( $\beta$ ) are listed. The dipole polarizability indirectly provides a measure of the extent of distortion of the electron density, and hence the response of the system under the effect of an external static electric field. As shown in **Table 7**, the calculated polarizability figures  $\alpha_{ij}$ , have non-zero values and are dominated by the diagonal components. The calculated polarizability of DCPDMP is equal to  $3.52 \times 10^{-23}$  and  $3.46 \times 10^{-23}$  esu by B3LYP with the basis sets 6-31G(d) and 631G(d,p) levels of DFT theory. The calculated dipole moment and hyperpolarizability values obtained from B3LYP with the basis sets 6-31G (d) and 6-31G(d,p) method are collected in **Table 7**. Urea is one of the prototypical molecules used in the study of the NLO properties of the molecular systems. Therefore, it is used frequently as a threshold value for comparative purposes. The first order hyperpolarizability of DCPDMP with B3LYP/6-31G(d) basis set is  $44.19 \times 10^{-30}$  esu which is 119 times greater than the value of urea ( $\beta_{\text{tot}} = 0.372 \times 10^{-30}$  esu). From the computation, the high values of the hyperpolarizability of DCPDMP are probably attributed to the nonlinear optical (NLO) property of the molecule. In addition, it is evident that the extent of charge transfer in terms of the HOMO–LUMO gap or the optical gap  $\Delta E$ , which, in turn, can be used to understand its effect on the  $\beta$  values.  $\Delta E$  is directly proportional to the extent of charge transfer. For a small optical gap, the charge transfer occurs easily, thus, giving a higher value of  $\beta$ . The source of charge transfer is thus controlled by the energy of the HOMO, whereas the acceptance of the charge is dominated by the LUMO energy. Small optical gap enhances the charge transfer, which, in turn, is reflected in the larger values of  $\alpha$  and  $\beta$ . There is an inverse relationship between the HOMO–LUMO energy gap and the first hyperpolarizability values for DCPDMP as expected.

### 3.7. Molecular electrostatic potential (MEP)

Molecular electrostatic potential has been found to be a very useful tool in the investigation of the correlation between molecular structures with its physiochemical property relationship, including biomolecules and drugs [46,47]. The MEP has been plotted for DCPDMP molecule at the B3LYP/6-31G(d,p) basis set as shown in **Fig. 8**. The MEP superimposed on top of the total energy density as a shell. Because of the usefulness feature to study reactivity given that an approaching electrophile will be attracted to negative regions (where the electron distribution effect is dominant). The different electrostatic potential values

of the surface are represented by different colors: red represents regions of most negative electrostatic potential, blue represents regions of most positive electrostatic potential, and green represents regions of zero potential. Potential increases in the order: red<orange<yellow<green<blue. In all cases, the shape of the electrostatic potential surface is influenced by the structure and charge density distributions in the molecule with sites close to the oxygen atom, showing regions of most negative electrostatic potential. In the present work, as can be seen from the **Fig. 8**, the calculated result shows that the negative potentials are mainly over the electron negative oxygen atoms (O17, O26 and O31). In addition, negative electrostatic potential regions are observed around the chlorine atoms (Cl7 and Cl12). Positive potentials are over the nucleophilic reactive hydrogen atoms. This result gives information for the region from where the compound can have intermolecular interaction. The MEP provides a visual representation of the chemically active sites and comparative reactivity of atoms. As we have mentioned earlier, the electrostatic potential has been used primarily for predicting sites and relative reactivity towards electrophilic attack, and in studies of biological recognition and hydrogen bonding interactions [48,49].

## Conclusion

Optimized geometrical parameters of the title compound were studied by density functional method and in agreement with the XRD data. Molecular structure and vibrational wavenumbers of the title compound were studied using vibrational spectra and density functional method. The DFT based calculations for the title compound is reproduced its experimental geometry and vibrational wavenumbers excellently. The wavenumbers proposed by the TED analysis are in good agreement with the observed wavenumbers. The NBO analysis reveals the reasons for hyper-conjugative interaction and stability of the molecule. A computation of the first hyperpolarizability of the compound indicates that this class of derivatives may be a good candidate as a NLO material. The HOMO and LUMO analysis is used to determine the charge transfer within the molecule. From the MEP, it is evident that the negative charge covers the C=O and C–O groups and the positive region is over the C–Cl group. To summarize, the following conclusions can be drawn:

- (1) The compound crystallizes in the triclinic space group P-1 with  $a = 7.6179 (7)$ ,  $b = 8.5023 (7)$ ,  $c = 12.1967 (10) \text{ \AA}$ ,  $V = 764.39 (11) \text{ \AA}^3$  and two molecules in the unit cell.
- (2) The HOMO is localized mainly on both the rings, while LUMO is localized carbonyl, methoxy, ethylenic bridge groups and benzene ring.

- (3) The first order hyperpolarizability of DCPDMP with B3LYP/6-31G(d) basis set is  $44.19 \times 10^{-30}$  esu which is 119 times greater than the value of urea ( $\beta_{\text{tot}} = 0.372 \times 10^{-30}$  esu). Therefore, we conclude that the title compound is an attractive object for future studies of nonlinear optical properties.
- (4) As can be seen from the MEP Figure, the negative potential surfaces are mainly over the electron negative oxygen atoms (O17, O26 and O31).

## References

- [1] Ch. Bosshard, R. Spreiter, L. Degiorgi, P. Gunter, *Phys. Rev.*, 66 (2002) 1–9.
- [2] B. Zhao, W.Q. Lu, Z.H. Zhou, Y.J. Wu, *Mater. Chem.*, 10 (2000) 1513–1515.
- [3] Y. Goto, A. Hayashi, Y. Kimura, M. Nakayama, *J. Crystal Growth.*, 108 (1991) 688–698.
- [4] B. Zhao, Y. Wu, Z.H. Zhou, W.Q. Lu, C.Y. Chen, *Appl. Phys.* 70 (2000) 601–605.
- [5] D. Wu, B. Zhao, Z. Zhou, *J. Mol. Struct.*, 83 (2004) 679–682.
- [6] A.M. Asiri, M. Karabacak, S. Sakthivel, A.O. Al-youbi, S. Muthu, S.A. Hamed, S. Renuga, T. Alagesan, *Journal of Molecular Structure* 1103 (2016) 145-155
- [7] M.J. Frisch et al., *Gaussian 09, C3 Revision B.01*, Gaussian, Inc., Wallingford, CT, 2010.
- [8] M.H. Jamroz, *Vibrational Energy Distribution Analysis, VEDA 4 Computer Program*, Poland, 2004.
- [9] E.D. Glendening, J.K. Badenhoop, A.E. Reed, J.E. Carpenter, J.A. Bohmann, C.M. Morales, F. Weinhold, *NBO 5.0*, Theoretical Chemistry Institute, University of Wisconsin, Madison, 2001.
- [10] Bruker. APEX2, SAINT and SADABS. Bruker AXS Inc., Madison, Wisconsin, USA. 2009.
- [11] G.M. Sheldrick, A Short History of SHELX. *Acta Cryst.* A64 (2008) 112-122.
- [12] J. Bernstein, R.E. Davis, L. Shimoni, N.L. Chang, *Angew. Chem. Int. Ed. Engl.* 34, (1995) 1555–1573.
- [13] H.K. Fun, S.I.J. Asik, P.L. Lobo, D. J. Prasad, *Acta Cryst.* E67 (2011) o2403.
- [14] Z. Li, Y. Wang, K. Peng, L. Chen and S. Chu. *Acta Cryst.* E68 (2012) o776.
- [15] B. Umesha, Y.B. Basavaraju, M. Kaur, H.S. Yathirajan, J.P. Jasinski. *Acta Cryst.* E70 (2014) o368.
- [16] G. Socrates, *Infrared and Raman Characteristic Group Frequencies-Tables and Charts*, Fourth ed., J. Wiley & Sons, Chichester, 2004.

- [17] M. Karabacak, D. Karagöz, M. Kurt, *Spectrochim. Acta A*, 72 (2009) 1076-1083.
- [18] M. Kurt, P. Chinna Babu, N. Sundaraganesan, M. Cinar, M. Karabacak, *Spectrochim. Acta A*, 79 (2011) 1162-1170.
- [19] V. Krishnakumar, V. Balachandran, *Spectrochimica Acta A* 61 (2005) 1001–1006.
- [20] M. Govindarajan, M. Karabacak, S. Periandy, D.Tanuja, *Spectrochim. Acta A*, 97 (2012) 231-245.
- [21] M. Govindarajana, K. Ganasan, S. Periandy, M. Karabacak, S. Mohan, *Spectrochimica Acta A* 77 (2010) 1005–1013
- [22] N.B. Colthup, L.H. Daly, S.E. Wiberley, *Introduction to Infrared and Raman Spectroscopy*, Academic Press, New York, 1990.
- [23] B.C. Smith, *Infrared Spectral Interpretation: A Systematic Approach*, CRC Press, Boca Raton, FL, 1998.
- [24] M. Silverstein, G.C. Basseler, C. Morill, *Spectrometric Identification of Organic Compounds*, Wiley, New York, 1981.
- [25] G. Varsanyi, *Assignments for Vibrational Spectra of 700 Benzene derivatives*, Adam Hilger, London, 1974.
- [26] P.B. Nagabalasubramanian, M. Karabacak, S. Periandy, *Spectrochim. Acta A*, 85 (2012) 43-52
- [27] M. Kumru, V. Küçük, M. Kocademir, H.M. Alfanda, A. Altun, L. Sarı, *Spectrochim. Acta A*, 134 (2015) 81-89.
- [28] P.B. Nagabalasubramanian, M. Karabacak, S. Periandy, *Spectrochim. Acta A*, 82 (2011) 169-180.
- [29] A. Coruh, F. Yilmaz, B. Sengez, M. Kurt, M. Cinar, M. Karabacak, *Structural Chemistry*, 22 (2011) 45-56.
- [30] G. Gece, *Corros. Sci.* 50 (2008) 2981–2992.
- [31] D. Lewis, C. Ioannides, D. Parke, *Xenobiotica* 24 (1994) 401–408.
- [32] Y. Uesugi, M. Mizuno, A. Shimojima, H. Takahashi, *J. Phys. Chem.* 101 (1997) 268–274.
- [33] L. Padmaja, C.R. Kumar, D. Sajan, I.H. Joe, V. Jayakumar, G. Pettit, *J. Raman Spectrosc.* 40 (2009) 419–428.
- [34] .S. Sudha, N. Sundaraganesan, M. Kurt, M. Cinar, M. Karabacak, *Journal of Molecular Structure*, 985 (2011) 148-156
- [35] R.G. Parr, L. Szentpaly, S. Liu, *J. Am. Chem. Soc.* 121 (1999) 1922–1924.
- [36] P.K. Chattaraj, B. Maiti, U. Sarkar, *J. Phys. Chem. A*107 (2003) 4973–4975.

- [37] R.G. Parr, P.K. Chattraj, *J. Am. Chem. Soc.* 113 (1991) 1854–1855.
- [38] M. Szafran, A. Komasa, E.B. Adamska, *J. Mol. Struct. Theochem.* 827 (2007) 101–107.
- [39] M. Govindarajan, M. Karabacak, A.Suvitha, S. Periandy, *Spectrochim. Acta A*, 89 (2012) 137-148.
- [40] C. James, A. Amal Raj, R. Reghunathan, I.H. Joe, V.S. Jayakumar, *J. Raman Spectrosc.* 37 (2006) 138.
- [41] J.N. Liu, Z.R. Chen, S.F. Yuan, *J. Zhejiang Univ. Sci.* 6B (2005) 584–589.
- [42] C.R. Zhang, H.S. Chen, G.H. Wang, *Chem. Res. Chin. Univ.* 20 (2004) 640–643.
- [43] S. Sudha, M. Karabacak, M. Kurt, M. Cinar, N. Sundaraganesan, *Spectrochim. Acta A*, 84 (2011) 184-195.
- [44] O. Christiansen, J. Gauss, J.F. Stanton, *J. Chem. Phys. Lett.* 305 (1999)147–155.
- [45] R.T. Lynch Jr., M.D. Levenson, N. Bloembergen, *Phys. Lett. A* 50 (1974) 61–62.
- [46] J.S. Murray, K. Sen, *Molecular Electrostatic Potentials, Concepts and Applications*, Elsevier, Amsterdam, 1996.
- [47] E. Scrocco, J. Tomasi, *Adv. Quantum Chem.* 11 (1978) 115–121.
- [48] P. Politzer, J.S. Murray, Electrostatic potential analysis of dibenzo-p-dioxins and Structurally similar systems in relation to their biological activities, in: D.L. Beveridge, R.Lavery (Eds.), *Theoretical Biochemistry and Molecular Biophysics: A Comprehensive Survey, protein*, vol. 2, Adenine Press, Schenectady, NY, 1991.
- [49] P. Politzer, D.G. Truhler (Eds.), *Chemical Applications of Atomic and Molecular Electrostatic Potentials*, Plenum Press, NY, 1981.

**Table 1.** Crystal data and parameters for structure refinement of the title compound.

<b>Compound</b>	<b>(I)</b>
Molecular formula	C <sub>17</sub> H <sub>14</sub> Cl <sub>2</sub> O <sub>3</sub>
Molecular weight	337.18
Crystal system	Triclinic
Space group	<i>P</i> -1
<i>a</i> (Å)	7.6179 (7)
<i>b</i> (Å)	8.5023 (7)
<i>c</i> (Å)	12.1967 (10)
$\alpha$ (°)	93.2313 (19)
$\beta$ (°)	98.0150 (17)
$\gamma$ (°)	101.2475 (18)
<i>V</i> (Å <sup>3</sup> )	764.39 (11)
<i>Z</i>	2
D <sub>calc.</sub> (g cm <sup>-3</sup> )	1.465
Crystal dimensions (mm)	0.48 × 0.20 × 0.12
$\mu$ (mm <sup>-1</sup> )	0.43
Radiation $\lambda$ (Å)	0.71073
Reflections measured	12215
Ranges/ indices ( <i>h, k, l</i> )	-9, 9; -10, 10; -15, 15
$\theta$ limit (°)	1.7-26.0
Unique reflections	2986
Observed reflections	2459
( <i>I</i> > 2 $\sigma$ ( <i>I</i> ))	
Parameters	201
Goodness of fit on <i>F</i> <sup>2</sup>	1.09
R1, wR2 ( <i>I</i> ≥ 2 $\sigma$ ( <i>I</i> ))	0.043; 0.135

**Table 2.** Hydrogen-bond geometry of the title compound

<i>D—H···A</i>	<i>D—H</i>	<i>H···A</i>	<i>D···A</i>	<i>D—H···A</i>
C9—H9A···C11	0.93	2.46	2.982 (3)	115
C8—H8A···C12	0.93	2.51	3.146(2)	125
C13—H13A···O1i	0.93	2.45	3.338(3)	160
C(17)—H(17C)···Cg(1)ii	0.96	2.83	3.714(3)	153

Symmetry codes: (i)  $x+1, y+1, z+1$ ; (ii)  $-x, -y+1, -z$ .

**Table 3.** Comparison of the geometrical parameters of DCPDMP, bond length (Å) in angstrom and bond angles (°) in degrees by using B3LYP/6-31G(d) and B3LYP/6-31G(d,p) level.

Bond Lengths	Exp	6-31G(d)	6-31G(d,p)	Bond Angles	Exp	6-31G(d)	6-31G(d,p)	Bond Angles (dihedral)	Exp	6-31G(d)	6-31G(d,p)
C1–C2	1.41	1.42	1.42	C16–C18–C19	120.0	120.2	120.5	C3–C4–C5–H10	-	179.1	179.1
C1–C6	1.41	1.41	1.41	C16–C18–C23	120.2	119.7	119.2	H9–C4–C5–C6	-	179.9	179.8
C1–C11	-	1.47	1.47	C19–C18–C23	120.0	120.1	120.3	H9–C4–C5–H10	-	-0.6	-0.6
C2–C3	1.38	1.39	1.39	C18–C19–C20	124.5	124.3	124.3	C4–C5–C6–C1	-0.7	0.1	0.1
C2–C17	1.74	1.83	1.76	C18–C19–H24	116.8	117.0	116.7	C4–C5–C6–Cl12	178.8	177.8	177.9
C3–C4	1.37	1.40	1.39	C20–C19–H24	118.7	118.7	119.1	H10–C5–C6–C1	-	-179.4	-179.5
C4–C5	1.37	1.40	1.39	C19–C20–C21	120.9	120.0	119.9	H10–C5–C6–Cl12	-	-1.7	-1.7
C5–C6	1.38	1.39	1.39	C19–C20–H25	119.5	121.4	121.3	C1–C11–C14–H15	-	0.1	0.1
C6–Cl12	-	1.83	1.76	C21–C20–H25	119.5	118.5	118.6	C1–C11–C14–C16	176.1	179.0	178.6
C11–H13	0.93	1.09	1.09	C20–C21–C22	119.9	121.3	121.2	H13–C11–C14–H15	-	-177.0	-176.7
C11–C14	1.30	1.35	1.34	C20–C21–O26	119.5	121.3	121.2	H13–C11–C14–C16	-	1.9	1.8
C14–H15	0.93	1.08	1.08	C22–C21–O26	120.1	117.3	117.6	C11–C14–C16–O17	-5.9	2.9	2.9
C14–C16	1.49	1.48	1.49	C21–C22–C23	119.7	118.9	119.3	C11–C14–C16–C18	173.3	-176.8	-176.7
C16–O17	1.21	1.26	1.23	C21–C22–O31	114.6	115.5	118.0	H15–C14–C16–O17	-	-178.2	-178.6
C16–C18	1.49	1.49	1.50	C23–C22–O31	125.7	125.5	122.7	H15–C14–C16–C18	-	2.1	1.8
C18–C19	1.38	1.41	1.40	C18–C23–C22	119.7	119.6	119.3	C14–C16–C18–C19	-	-1.6	-2.7
C18–C23	1.40	1.41	1.41	C18–C23–H36	114.9	116.8	116.2	C14–C16–C18–C23	-	178.0	177.0
C19–C20	1.39	1.39	1.39	C22–C23–H36	125.3	123.6	124.5	O17–C16–C18–C19	-	178.7	177.6
C20–C21	1.38	1.40	1.39	C21–O26–C27	121.2	121.5	121.3	O17–C16–C18–C23	-	-1.7	-2.7
C21–C22	1.41	1.42	1.42	O26–C27–H28	119.4	117.0	117.0	C16–C18–C19–C20	-	-179.6	-179.5
C21–O26	1.35	1.38	1.37	O26–C27–H29	119.4	121.6	121.7	C16–C18–C19–H24	-	-0.5	-0.4
C22–C23	1.37	1.39	1.39	O26–C27–H30	118.2	122.1	117.4	C23–C18–C19–20	-	0.7	0.8
C22–O31	1.37	1.39	1.37	H28–C27–H29	109.5	104.2	105.7	C23–C18–C19–H24	-	179.9	179.9
C23–H36	0.93	1.08	1.08	H28–C27–H30	109.5	111.1	111.7	C16–C18–C23–C22	-	-179.6	-179.6
O26–C27	1.43	1.47	1.43	H29–C27–H30	109.5	110.7	110.6	C16–C18–C23–H36	-	-0.4	-0.5
O31–C32	1.42	1.45	1.42	C22–O31–C32	109.5	111.1	109.9	C19–C18–C23–C22	-	0.1	0.1
C–H Ring average	0.93	1.08	1.08	O31–C32–H33	109.5	110.1	109.2	C19–C18–C23–H36	-	179.2	179.2
C–H Methyl average	0.96	1.09	1.10	O31–C32–H34	-	109.6	109.6	C18–C19–C20–C21	-	-0.4	-0.6
<b>Bond Angles</b>	<b>Exp</b>	<b>6-31G(d)</b>	<b>6-31G(d,p)</b>	O31–C32–H35	-	118.4	117.9	C18–C19–C20–H25	-	179.4	179.6
C6–C1–C11	-	114.4	115.2	H33–C32–H34	-	111.0	111.4	H24–C19–C20–C21	-	-179.6	-179.7

C1-C2-C3	118.7	119.6	119.3	H33-C32-H35	-	111.2	111.6	H24-C19-C20-H25	-	0.2	0.5
C1-C2-C17	126.9	126.0	125.5	H34-C32-H35	-	105.0	105.8	C19-C20-C21-C22	-	-0.7	-0.6
C3-C2-C17	123.5	123.9	123.2	<b>Bond Angles</b>	<b>Exp</b>	<b>6-31G(d)</b>	<b>6-31G(d,p)</b>	C19-C20-C21-O26	-	-177.7	-176.9
C2-C3-C4	120.0	119.6	119.7	C6-C1-C2-C3	-1.6	-0.8	-0.9	H25-C20-C21-C22	-	179.5	179.3
C2-C3-H8	116.5	116.5	117.1	C6-C1-C2-C17	178.5	-179.6	-179.5	H25-C20-C21-O26	-	2.4	2.9
C4-C3-H8	-	119.1	119.3	C11-C1-C2-C3	178.2	-179.1	-178.9	C20-C21-C22-C23	-	1.5	1.5
C3-C4-C5	120.4	119.8	119.6	C11-C1-C2-C17	-1.7	2.1	2.5	C20-C21-C22-O31	-	-177.6	-177.6
C3-C4-H9	120.4	121.1	121.2	C2-C1-C6-C5	1.8	0.5	0.5	O26-C21-C22-C23	-	178.2	177.6
C5-C4-H9	-	119.8	120.0	C2-C1-C6-C112	-177.7	-177.1	-177.1	O26-C21-C22-O31	-	-0.8	-1.5
C4-C5-C6	120.0	120.1	120.0	C11-C1-C6-C5	-177.9	178.7	178.4	C20-C21-O26-C27	-	-148.8	-122.3
C4-C5-H10	120.0	120.1	120.0	C11-C1-C6-C112	2.5	1.1	0.7	C22-C21-O26-C27	-	34.3	61.6
C6-C5-H10	120.2	119.6	119.8	C2-C1-C11-H13	-	32.8	34.8	C21-C22-C23-C18	-	-1.2	-1.3
C1-C6-C5	119.9	120.7	120.9	C2-C1-C11-C14	-168.9	-144.3	-142.0	C21-C22-C23-H36	-	179.7	179.7
C1-C6-C112	119.9	119.5	119.3	C6-C1-C11-H13	-	-145.3	-142.9	O31-C22-C23-C18	-	177.8	177.8
C5-C6-C112	122.6	123.3	122.6	C6-C1-C11-C14	10.9	37.6	40.2	O31-C22-C23-H36	-	-1.2	-1.3
C1-C11-H13	121.1	121.4	121.4	C1-C2-C3-C4	-	0.5	0.6	C21-C22-O31-C32	-	178.8	178.1
C1-C11-C14	116.4	115.3	116.0	C1-C2-C3-H8	-	-179.3	-179.2	C23-C22-O31-C32	-	-0.2	-0.9
H13-C11-C14	112.9	115.8	116.0	C17-C2-C3-C4	-179.8	179.4	179.3	C21-O26-C27-H28	-	165.5	-
C11-C14-H15	-	127.9	127.9	C17-C2-C3-H8	-	-0.5	-0.6	C21-O26-C27-H29	-	-74.9	-65.5
C11-C14-C16	112.9	116.2	116.1	C2-C3-C4-C5	1.1	0.2	0.1	C21-O26-C27-H30	-	47.2	57.0
H15-C14-C16	120.1	121.3	121.2	C2-C3-C4-H9	-	179.8	179.8	C22-O31-C32-H33	-	-60.6	-60.0
C14-C16-O17	119.9	119.8	119.4	H8-C3-C4-C5	-	-180.0	179.9	C22-O31-C32-H34	-	61.7	62.2
C14-C16-C18	-	118.9	119.4	H8-C3-C4-H9	-	-0.3	-0.3	C22-O31-C32-H35	-	-179.4	-178.9
O17-C16-C18	120.1	-	-	C3-C4-C5-C6	-0.8	-0.5	-0.5				

Numbering of atoms is adopted from Gaussian in Fig. 4

**Table 4.** Comparison of the experimental (FT-IR and FT-Raman) and theoretical wavenumbers ( $\text{cm}^{-1}$ ) of DCPDMP calculated by B3LYP/6-31G(d) and B3LYP/6-31G(d,p) level.

No.	FT-IR	FT-Raman	Unscaled		Scaled		TED (%) among types of internal coordinates
			6-31G(d)	6-31G(d,p)	6-31G(d)	6-31G(d,p)	
1		3113	3254	3275	3166	3115	vC14-H15(91)
2	3109		3239	3253	3135	3110	vC23-H36(99)
3			3231	3252	3113	3088	vC3-H8(47), vC5-H10(36), vC4-H9(16)
4		3081	3226	3247	3107	3079	vC5-H10(55), vC3-H8(45)
5	3078		3223	3243	3091	3076	vC19-H24(68), vC20-H25(24)
6			3207	3226	3080	3036	vC20-H25(75), vC19-H24(24)
7			3204	3223	3047	3014	vC4-H9(83)
8	3005		3188	3200	3026	3005	vC11-H13(99)
9		3000	3157	3197	3018	3001	vC27-H28(59), vC27-H29(40)
10			3154	3184	3007	2989	vC32-H35(89)
11			3122	3163	2996	2981	vC27-H29(45), vC27-H28(27), vC27-H30(26)
12	2962		3092	3118	2983	2960	vC32-H33(52), vC32-H34(47)
13	2937	2936	3034	3068	2955	2935	vC27-H30(72), vC32-H34(47), vC27-H28(13)
14	2841	2836	3026	3044	2867	2842	vC32-H34(47), vC32-H33(41), vC32-H35(10)
15		1661	1741	1709	1683	1660	vO17-C16(60), vC11-C14(19)
16	1650		1671	1656	1671	1650	vC11-C14(45), vO17-C16(21)
17			1645	1641	1653	1627	vC22-C23(28), vC20-C21(11)
18	1591		1632	1628	1618	1593	vC2-C3(28), vC5-C6(20)
19	1575		1621	1602	1593	1574	vC18-C19(20), vC21-C22(20), $\delta$ H9-C4-C5(15), vC20-C21(15)
20		1565	1603	1599	1586	1565	vC3-C4(29), vC4-C5(20), vC1-C2(20), vC1-C6(10)
21		1516	1553	1563	1547	1515	$\delta$ H25-C20-C19(13), vC21-C22(20), $\delta$ H36-C23-C18(11), vO26-C21(10), vO26-C21(10)
22	1511		1527	1544	1531	1514	$\delta$ H29-C27-H30(73), $\gamma$ C27-H28-O26-H29(12)
23	1487		1518	1538	1508	1485	$\delta$ H33-C32-H34(61), $\delta$ H34-C32-H35(15), $\gamma$ C32-H33-O31-H34(11), $\delta$ H33-C32-H35(10)
24			1504	1533	1490	1470	$\delta$ H34-C32-H35(42), $\gamma$ C32-H34-O31-H35(14)
25	1458		1501	1525	1481	1459	$\gamma$ C27-H28-O26-H30(19), $\delta$ H28-C27-H30(15), $\delta$ H33-C32-H35(11), $\delta$ H33-C32-H34(10)

26			1496	1506	1469	1443	$\delta$ H28-C27-H30(52), $\delta$ H34-C32-H35(12), $\delta$ H29-C27-O26(11)
27	1435	1436	1480	1495	1451	1435	$\delta$ H29-C27-O26(27), $\gamma$ C27-H28-O26-H30(26), $\delta$ H28-C27-H30(14)
28			1472	1490	1446	1428	$\delta$ H10-C5-C4(30), $\nu$ C1-C6(19), $\delta$ H9-C4-C5(14)
29	1418	1419	1463	1480	1435	1420	$\delta$ H8-C3-C2(30), $\nu$ C1-C2(15), $\delta$ H9-C4-C5(10)
30		1355	1452	1464	1371	1355	$\nu$ C22-C23(22), $\nu$ C19-C20(11), $\delta$ H24-C19-C18(15)
31	1327		1368	1398	1358	1328	$\nu$ C18-C19(17), $\nu$ C21-C22(15), $\delta$ H15-C14-C11(13), $\nu$ C20-C21(12)
32	1309		1360	1383	1333	1310	$\delta$ H15-C14-C11(29), $\delta$ H13-C11-C1(13), $\nu$ C20-C21(12), $\nu$ C11-C14(11)
33	1296		1341	1370	1318	1293	$\delta$ H13-C11-C1(36), $\delta$ H15-C14-C11(11)
34			1315	1341	1290	1274	$\nu$ O31-C22(52), $\delta$ H36-C23-C18(13)
35		1258	1308	1328	1286	1260	$\nu$ O26-C21(21), $\nu$ H24-C19-C18(11), $\nu$ H25-C20-C19(16)
36	1253		1298	1308	1266	1251	$\delta$ H36-C23-C18(17), $\delta$ H24-C19-C18(12), $\delta$ H13-C11-C1(10)
37		1242	1264	1285	1260	1245	$\nu$ O26-C21(14), $\delta$ H36-C23-C18(11), $\delta$ O31-C22(10)
38		1226	1249	1269	1237	1224	$\nu$ C5-C6(30), $\delta$ H10-C5-C4(28), $\nu$ C1-C11(16)
39		1210	1223	1231	1231	1210	$\gamma$ C32-H33-O31-H34(53), $\nu$ C16-C18(10)
40	1194		1211	1222	1217	1195	$\gamma$ C27-H28-O26-H30(23), $\gamma$ C27-H28-O26-H29(21), $\nu$ C1-C2(13), $\nu$ C2-C3(10)
41	1183		1206	1204	1208	1182	$\delta$ H8-C3-C29(35), $\nu$ C1-C2(13), $\nu$ C2-C3(10)
42		1177	1193	1199	1191	1175	$\gamma$ C32-H33-O31-H34(16), $\delta$ H36-C23-C18(10), $\nu$ C16-C18(11)
43		1161	1178	1194	1188	1160	$\delta$ H9-C4-C5(43), $\nu$ C16-C18(10)
44	1151		1178	1169	1169	1153	$\gamma$ C32-H34-O31-H35(78), $\delta$ H33-C32-H35(14), $\nu$ C4-C5(10)
45		1145	1176	1165	1158	1144	$\gamma$ C27-H28-O26-H29(38), $\delta$ H29-C27-O26(36)
46		1096	1157	1158	1131	1095	$\delta$ H25-C20-C19(29), $\delta$ H24-C19-C18(24), $\nu$ C19-C20(17)
47		1065	1107	1115	1093	1066	$\nu$ C3-C4(32), $\nu$ C4-C5(31), $\delta$ H10-C5-C4(10), $\delta$ H8-C3-C2(10)
48	1052		1091	1092	1083	1053	$\delta$ C1-C6-C5(24), $\delta$ C4-C5-C6(17), $\delta$ C3-C4-C5(13)
49		1032	1075	1090	1051	1030	$\nu$ C18-C23(16), $\nu$ C14-C16(15), $\delta$ H36-C23-C18(13), $\nu$ C18-C19(10)
50	1026		1064	1042	1037	1025	$\nu$ O31-C32(54)
51	1014		1040	1028	1028	1015	$\nu$ O26-C27(69), $\tau$ H15-C14-C11-C1(12)
52		1000	1021	1019	1016	1002	$\gamma$ C11-C1-C14-H13(73), $\tau$ H15-C14-C11-C1(22)
53	978		979	996	991	975	$\tau$ H9-C4-C5-H10(79), $\tau$ H8-C3-C2-C17(11)
54			940	975	970	956	$\tau$ H25-C20-C21-O26(58), $\tau$ H24-C19-C18-C16(25)
55	917	919	937	960	937	920	$\nu$ C14-C16(21), $\delta$ C11-C14-C16(13)
56			918	947	906	893	$\tau$ H36-C23-C18-C16(83)
57	884		908	946	893	880	$\tau$ H8-C3-C2-C17(50), $\gamma$ C5-C4-C6-H10(38)

58	871	887	929	888	870	$\tau$ H15-C14-C11-C1(47), $\gamma$ C11-C1-C14-H13(10)
59	855	879	887	871	856	$\nu$ C3-C4-C5(17)
60	841	833	855	864	842	$\tau$ H24-C19-C18-C16(51), $\tau$ H25-C20-C21-O26(30)
61	813	790	820	831	815	$\delta$ C19-C18-C23(14), $\delta$ C3-C4-C5(11)
62	774	789	795	783	775	$\gamma$ C5-C4-C6-H10(41), $\tau$ H8-C3-C2-C17(24)
63	767	779	779	771	764	$\nu$ C17-C2(24), $\nu$ C4-C5-C6(22), $\nu$ Cl12-C6(17)
64	758	772	758	764	758	$\nu$ C21-C22(11), $\nu$ O31-C22(11)
65	742	753	755	758	740	$\gamma$ O17-C14-C18-C16(22), $\tau$ C1-C6-C5-C4(11), $\gamma$ C19-C16-C23-C18(10)
66	734	729	742	746	733	$\tau$ C19-C20-C21-C22(24), $\tau$ O26-C21-C22-O31(22)
67	685	702	712	693	684	$\gamma$ O17-C14-C18-C16(22), $\tau$ C1-C6-C5-C4(15), $\tau$ C1-C2-C3-C4(12)
68	645	653	662	653	640	$\delta$ C19-C20-C21(27)
69	601	610	616	606	600	$\delta$ C14-C16-O17(22)
70	584	588	590	588	581	$\gamma$ C19-C16-C23-C18(49), $\tau$ O26-C21-C22-O31(10)
71	565	581	579	570	562	$\delta$ C20-C21-O26(19), $\delta$ C16-C18-C23(10)
72	557	558	566	561	553	$\delta$ C18-C19-C20(18), $\delta$ C14-C16-C18(11), $\tau$ C3-C4-C5-C6(10)
73	532	539	549	544	530	$\tau$ C1-C6-C5-C4(26), $\gamma$ Cl7-C1-C3-C2(19), $\tau$ C2-C1-C6-Cl12(10)
74	521	538	544	530	522	$\gamma$ Cl7-C1-C3-C2(17), $\tau$ C1-C6-C5-C4(11)
75	491	517	528	495	490	$\tau$ C3-C4-C5-C6(37), $\delta$ C2-C1-C11(12)
76	463	466	501	489	462	$\gamma$ O31-C21-C23-C22(46), $\delta$ C21-O26-C27(11), $\tau$ C19-C20-C21-C22(13)
77	420	452	451	430	421	$\delta$ C22-O31-C32(21), $\delta$ C14-C16-C18(19)
78	404	420	413	410	403	$\nu$ Cl7-C2(26), $\delta$ C4-C5-C6(18), $\delta$ C1-C6-C5(12)
79	356	397	391	359	355	$\delta$ C5-C6-Cl12(23), $\nu$ Cl12-C6(17)
80		393	384	352	347	$\delta$ C21-O26-C27(15), $\tau$ C19-C20-C21-C22(11), $\tau$ C16-C18-C19-C20(10)
81		352	346	343	333	$\delta$ C1-C2-C17(19), $\delta$ C11-C14-H15(10)
82		333	328	328	320	$\delta$ C22-O31-C32(24), $\delta$ C20-C21-O26(17), $\delta$ C18-C19-C20(11)
83		320	324	316	311	$\tau$ C1-C11-C14-C16(19), $\tau$ C5-C6-C1-C11(19), $\delta$ C1-C2-C17(14)
84	308	303	313	310	306	$\delta$ C21-O26-C27(11), $\tau$ H33-C32-O31-C22(10), $\tau$ C16-C18-C19-C20(10)
85	228	273	267	230	226	$\tau$ H33-C32-O31-C22(51)
86		252	250	216	212	$\delta$ C1-C2-C17(17), $\delta$ C5-C6-Cl12(15), $\delta$ C11-C14-C16(11), $\tau$ H33-C32-O31-C22(10)
87		238	237	196	193	$\delta$ C5-C6-Cl12(19), $\delta$ C21-O26-C27(11)
88		213	215	184	180	$\delta$ C23-C22-O31(21), $\delta$ C20-C21-O26(14), $\delta$ C22-O31-C32(10)
89		201	202	168	166	$\tau$ C1-C2-C3-C4(46), $\tau$ C2-C1-C6-Cl12(26), $\tau$ C3-C4-C5-C6(10)

90		190	194	166	163	$\tau$ C16-C18-C23-C22(26)
91		181	180	154	151	$\tau$ C16-C18-C23-C22(13)
92	148	161	162	149	145	$\tau$ H28-C27-O26-C21(52)
93		136	141	130	126	$\tau$ C6-C1-C11-C14(16), $\delta$ C16-C18-C23(14), $\delta$ C23-C22-O31(10)
94		113	119	115	110	$\tau$ C6-C1-C11-C14(22), $\tau$ C11-C14-C16-C18(17), $\tau$ O26-C21-C22-O31(11)
95		97	97	95	93	$\tau$ C21-C22-O31-C32(57)
96		93	96	86	85	$\tau$ C1-C11-C14-C16(47), $\delta$ C2-C1-C11(12)
97		79	87	79	78	$\tau$ C6-C1-C11-C14(16), $\tau$ C16-C18-C19-C20(15), $\tau$ O26-C21-C22-O31(12)
98		62	63	63	60	$\tau$ C5-C6-C1-C11(31), $\tau$ C2-C1-C6-C11(15), $\tau$ C1-C11-C14-C16(16)
99		57	40	42	40	$\tau$ C22-C21-O26-C27(48), $\tau$ C5-C6-C1-C11(12)
100		36	36	34	33	$\delta$ C1-C11-C14(33), $\delta$ C11-C14-C16(20), $\tau$ C5-C6-C1-C11(12), $\gamma$ C14-C16-C18(10)
101		18	20	16	15	$\tau$ C14-C16-C18-C23(35), $\tau$ C11-C14-C16-C18(32), $\tau$ C6-C1-C11-C14(13)
102		9	12	9	8	$\tau$ C14-C16-C18-C23(48), $\tau$ C11-C14-C16-C18(33), $\tau$ C5-C6-C1-C11

v-stretching;  $\delta$ -in-plane deformation;  $\gamma$ -out-of-plane deformation;  $\tau$ -torsion

**Table 5.** The HOMO and LUMO energy gap ionization potential, Electron affinity, Chemical Hardness, Electronegativity, Softness, Chemical potential, Global electrophilicity index values of DCPDMP at the B3LYP/6-31G(d) and B3LYP/6-31G(d,p) level

<b>Parameters</b>	<b>6-31G(d)</b>	<b>6-31G(d,p)</b>
$E_{\text{HOMO}}$	5.9179	6.0162
$E_{\text{LUMO}}$	2.3178	2.1676
$E_{\text{HOMO}} - E_{\text{LUMO}}$ gap	3.6001	3.8485
Ionization potential(I.P, eV)	5.9179	6.0162
Electron affinity(E.A, eV)	2.3178	2.1676
Chemical Hardness( $\eta$ , eV)	1.8001	1.9243
Electronegativity( $\chi$ , eV)	4.1179	4.0919
Softness(S,eV <sup>-1</sup> )	0.5555	0.5197
Chemical potential( $\mu$ , eV)	-4.1179	-4.0919
Global electrophilicity index( $\omega$ )	4.7101	4.3506

**Table 6.** The second order perturbation energies E(2) (kcal/mol) corresponding to the most important charge transfer interactions (donor-acceptor) for DCPDMP by B3LYP/6-31G(d,p) method.

Donor	ED(i)e	Acceptor(j)	ED(j)e	E(2)	E(i)-E(j)	F(i,j)
$\sigma$ (C2-C17)	1.9879	$\sigma^*$ (C1-C6)	0.0380	2.56	1.24	0.051
$\sigma$ (C2-C17)	1.9879	$\sigma^*$ (C3-C4)	0.0167	2.55	1.28	0.051
$\pi$ (C4-C5)	1.6537	$\pi^*$ (C1-C6)	0.0380	21.45	0.27	0.069
$\pi$ (C4-C5)	1.6537	$\pi^*$ (C2-C3)	0.3742	21.10	0.27	0.068
$\sigma$ (C6-C112)	1.9880	$\sigma^*$ (C1-C2)	0.0357	2.46	1.24	0.050
$\sigma$ (C6-C112)	1.9880	$\sigma^*$ (C4-C5)	0.0168	2.65	1.28	0.052
$\pi$ (C16-O17)	1.9657	$\pi^*$ (C11-C14)	0.0762	4.18	0.40	0.037
$\pi$ (C16-O17)	1.9657	$\pi^*$ (C18-C19)	0.3859	4.98	0.39	0.044
$\pi$ (C18-C19)	1.6562	$\pi^*$ (C16-O17)	0.2089	20.08	0.27	0.068
$\pi$ (C18-C19)	1.6562	$\pi^*$ (C20-C21)	0.2089	19.62	0.28	0.066
$\pi$ (C18-C19)	1.6562	$\pi^*$ (C22-C23)	0.3499	19.18	0.28	0.065
$\pi$ (C22-C23)	1.6822	$\pi^*$ (C18-C19)	0.3859	18.28	0.30	0.067
$\pi$ (C22-C23)	1.6822	$\pi^*$ (C20-C21)	0.3531	18.86	0.29	0.067
LP(3)C17	1.9249	$\pi^*$ (C2-C3)	0.3742	12.01	0.33	0.061
LP(2)C12	1.9694	$\sigma^*$ (C1-C6)	0.0380	4.60	0.85	0.056
LP(3)C12	1.9274	$\pi^*$ (C1-C6)	0.0380	12.35	0.32	0.062
LP(2)O17	1.8834	$\sigma^*$ (C14-C16)	0.0590	19.27	0.69	0.105
LP(2)O17	1.8834	$\sigma^*$ (C16-C18)	0.0625	18.87	0.70	0.104
LP(1)O26	1.9538	$\sigma^*$ (C21-C22)	0.0424	7.82	1.02	0.080
LP(2)O26	1.8876	$\pi^*$ (C20-C21)	0.2089	13.44	0.38	0.068
LP(2)O26	1.8876	$\sigma^*$ (C27-H30)	0.0171	5.90	0.79	0.063
LP(1)O31	1.9618	$\sigma^*$ (C22-C23)	0.0248	7.13	1.13	0.080
LP(2)O31	1.8443	$\pi^*$ (C22-C23)	0.3499	29.35	0.34	0.095
LP(2)O31	1.8443	$\sigma^*$ (C32-H33)	0.0188	5.25	0.75	0.058
LP(2)O31	1.8443	$\sigma^*$ (C32-H34)	0.0189	5.27	0.75	0.058
$\pi^*$ (C1-C6)	0.0380	$\pi^*$ (C4-C5)	0.3309	169.32	0.02	0.080
$\pi^*$ (C1-C6)	0.0380	$\pi^*$ (C11-C14)	0.0762	23.10	0.05	0.059
$\pi^*$ (C2-C3)	0.3742	$\pi^*$ (C4-C5)	0.3309	228.76	0.01	0.084
$\pi^*$ (C16-O17)	0.2089	$\pi^*$ (C11-C14)	0.0762	39.59	0.02	0.072
$\pi^*$ (C16-O17)	0.2089	$\pi^*$ (C18-C19)	0.3859	146.86	0.01	0.073

ED; Electron density

<sup>a</sup> E(2) means energy of hyper conjugative interaction (stabilization energy).

<sup>b</sup> Energy difference between donor and acceptor i and j NBO orbitals.

<sup>c</sup> F(i,j) is the Fock matrix element between i and j NBO orbitals.

**Table 7.** The mean polarizability ( $\alpha$ ), anisotropic polarizability ( $\Delta\alpha$ ), dipole moment ( $\mu$ ), first-order hyperpolarizability ( $\beta$ ) and optical gap ( $\Delta E_{H-L}$ ) values of DCPDMP by B3LYP/6-31G(d) and 6-31G(d,p) method.

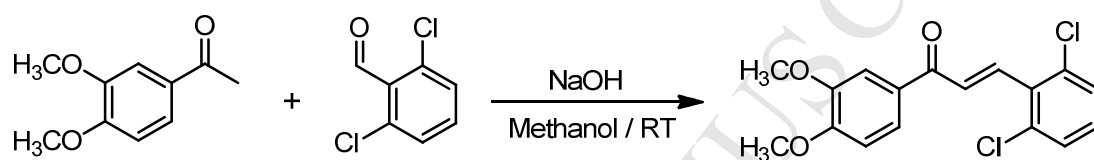
Parameters	6-31G(d)	6-31G(d,p)
$\alpha$ ( $\times 10^{-23}$ esu)	3.52	3.46
$\Delta\alpha$ ( $\times 10^{-23}$ esu)	4.25	3.48
$\mu$ (Debye)	0.8936	1.5648
$\beta$ ( $\times 10^{-30}$ esu)	44.19	21.9
$\Delta E_{H-L}$ (eV)	3.6001	3.8485

## Caption to Scheme

**Scheme 1:** Synthesis of (2E)-3-(2,6-dichlorophenyl)-1-(3,4-dimethoxyphenyl)prop-2-en-1-one.

## Captions to figures

- Fig. 1:** Molecular view of the compound, showing 50% probability displacement ellipsoids and atom labeling scheme.
- Fig. 2:** Crystal packing of the title compound, showing intermolecular C—H...O hydrogen bonding interactions and Cl...Cl short contacts as dotted lines. H atoms not involved in hydrogen bonding are omitted for clarity
- Fig. 3:** Crystal packing of the title compound, viewed along b axis
- Fig. 4:** The geometric structure of the title compound
- Fig. 5:** Observed and calculated infrared spectrum of the compound
- Fig. 6:** Observed and calculated Raman spectrum of the compound
- Fig. 7:** HOMO-LUMO plot of the title compound
- Fig. 8:** The molecular electrostatic potential surface of the title compound



**Scheme 1:** Synthesis of (2E)-3-(2,6-dichlorophenyl)-1-(3,4-dimethoxyphenyl)prop-2-en-1-one.

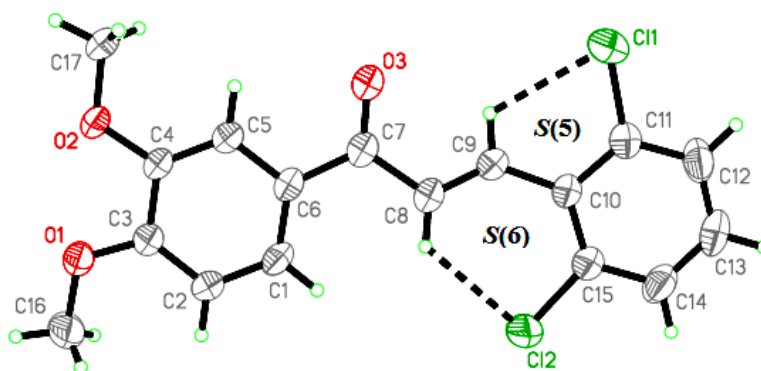


**Fig. 1:** Molecular view of compound, showing 50% probability displacement ellipsoids and atom labeling scheme.

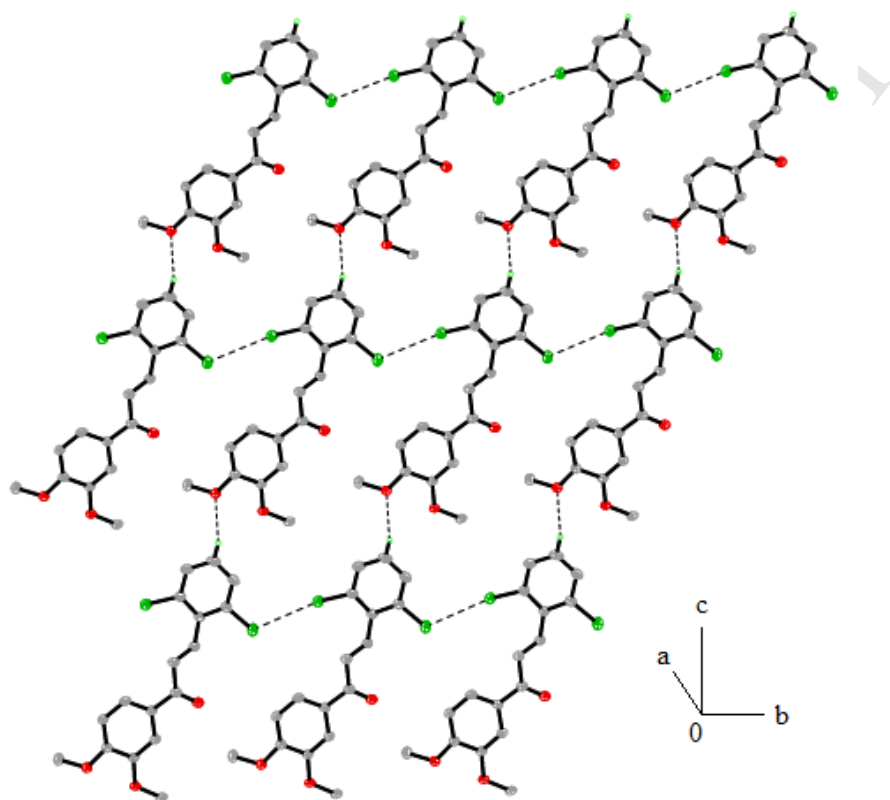


**Fig. 2:** Crystal packing of the title compound, showing intermolecular C—H $\cdots$ O hydrogen bonding interactions and Cl $\cdots$ Cl short contacts as dotted lines. H atoms not involved in hydrogen bonding are omitted for clarity

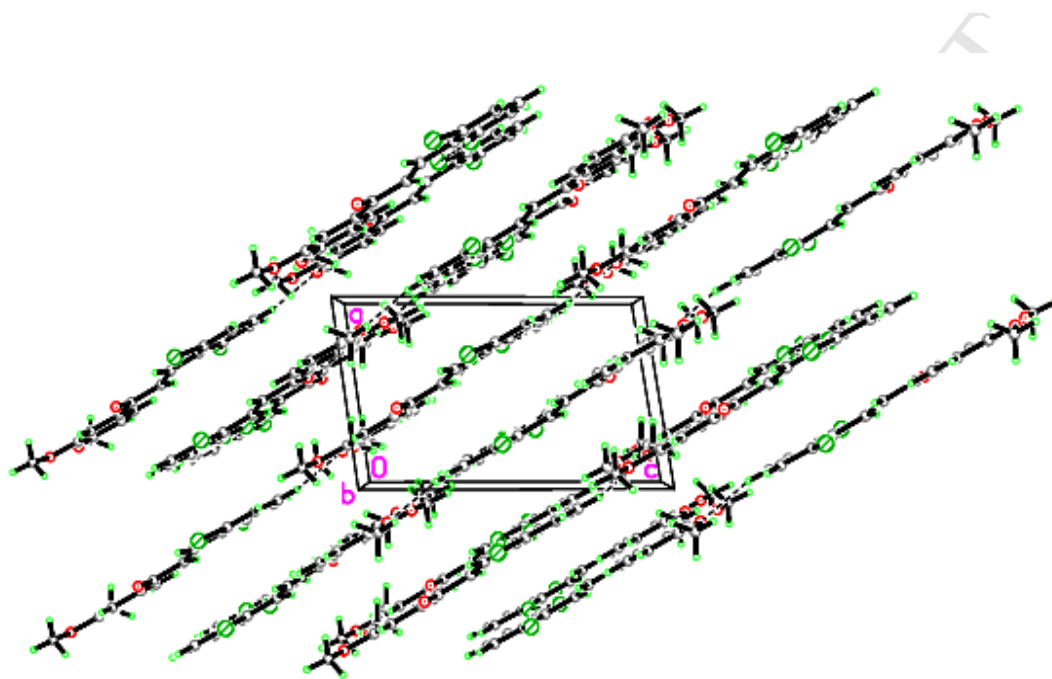


**Fig. 3:** Crystal packing of the title compound, viewed along  $b$  axis

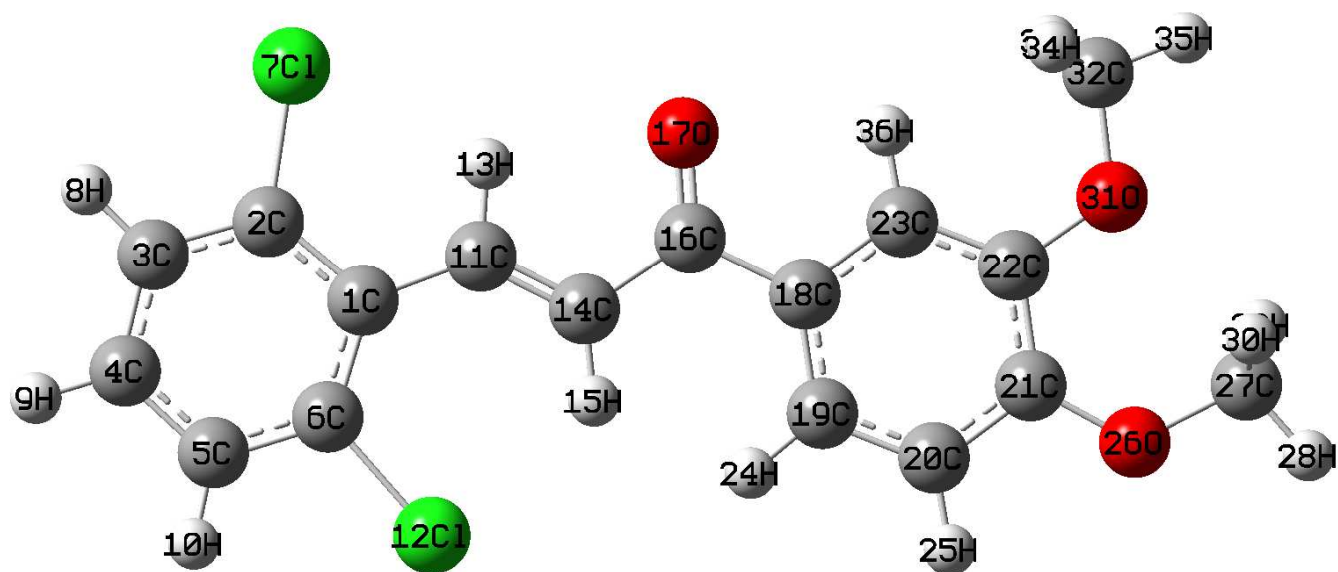


**Fig 4.** The geometric structure of the title compound

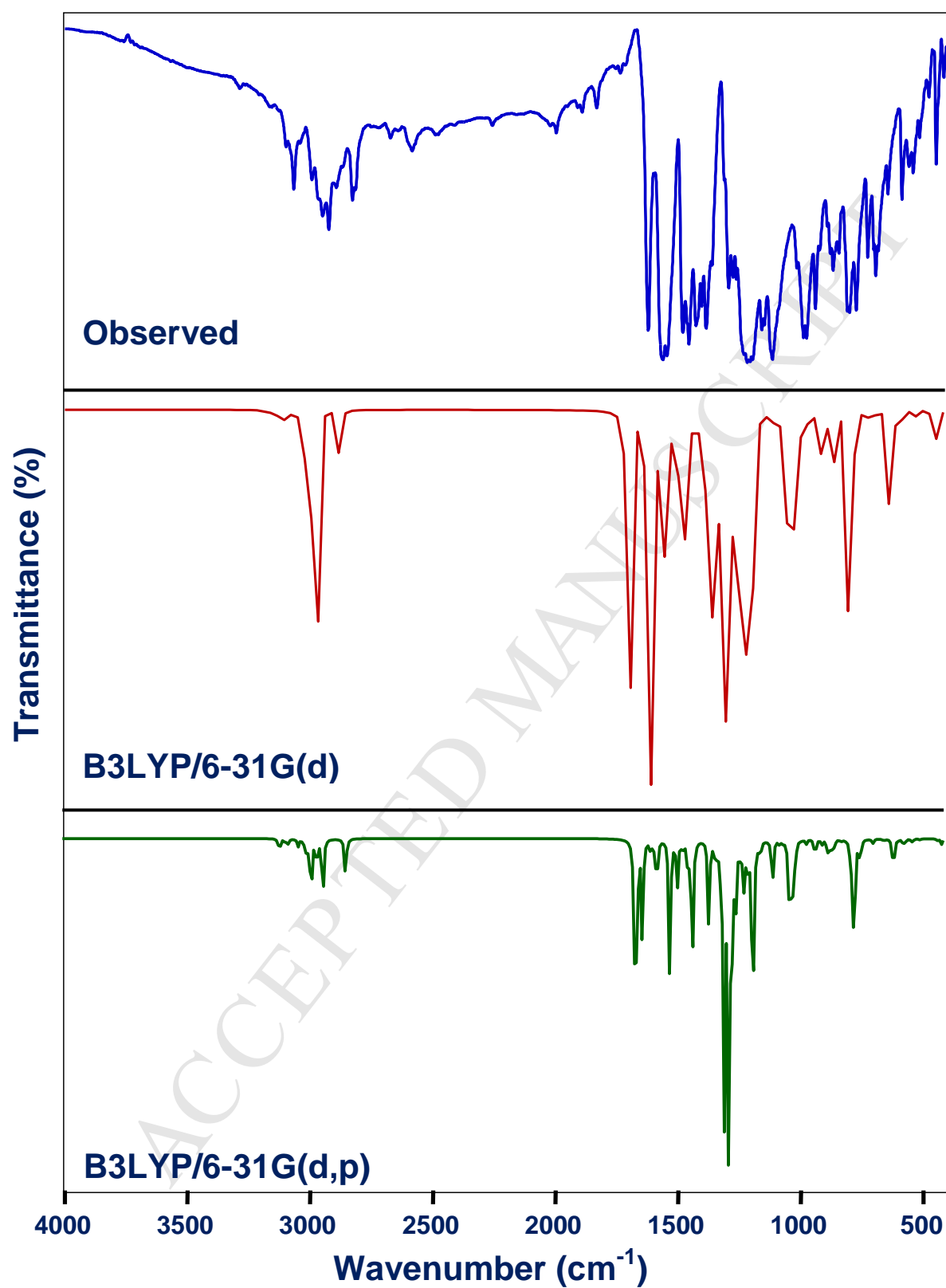
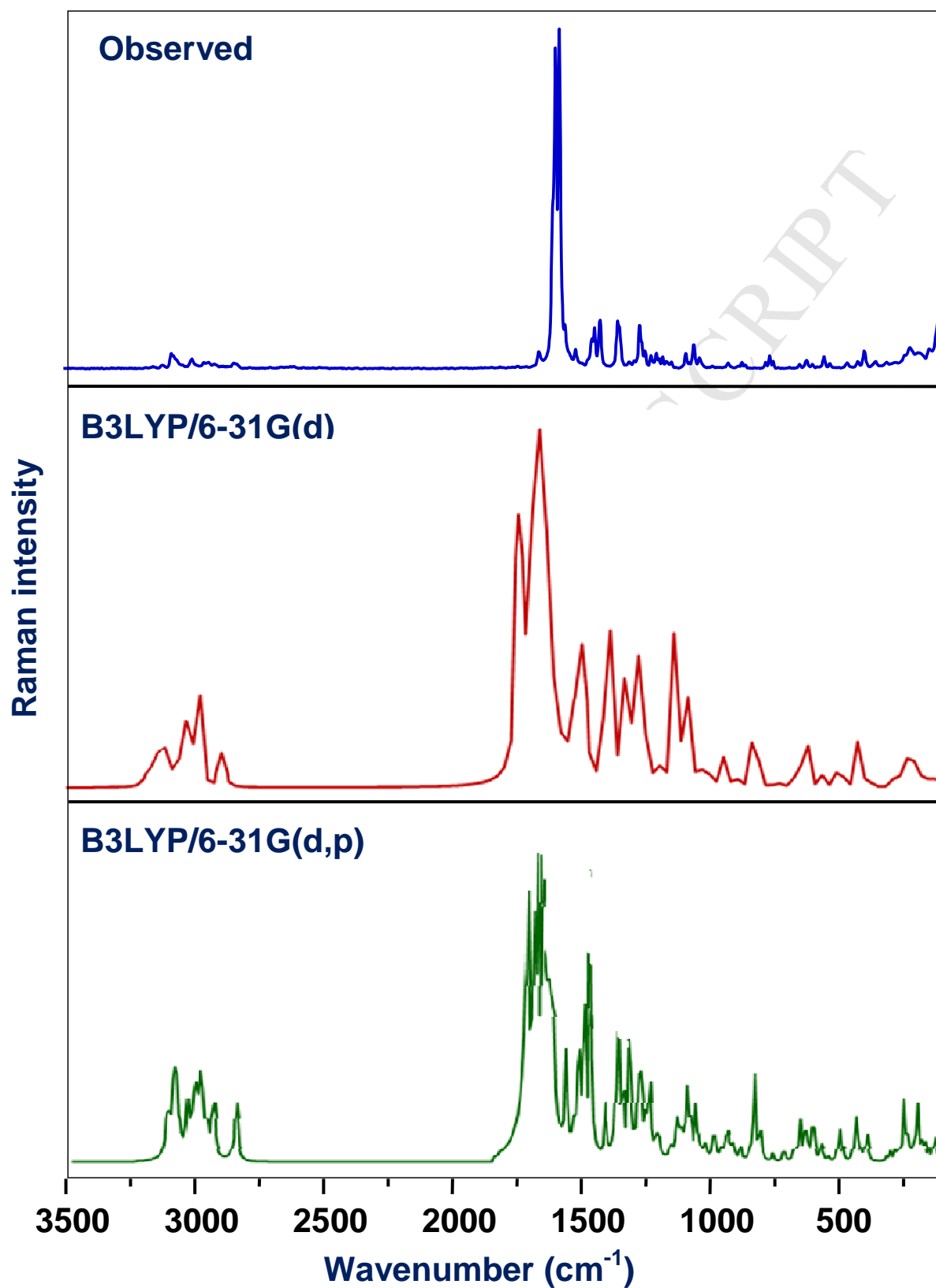
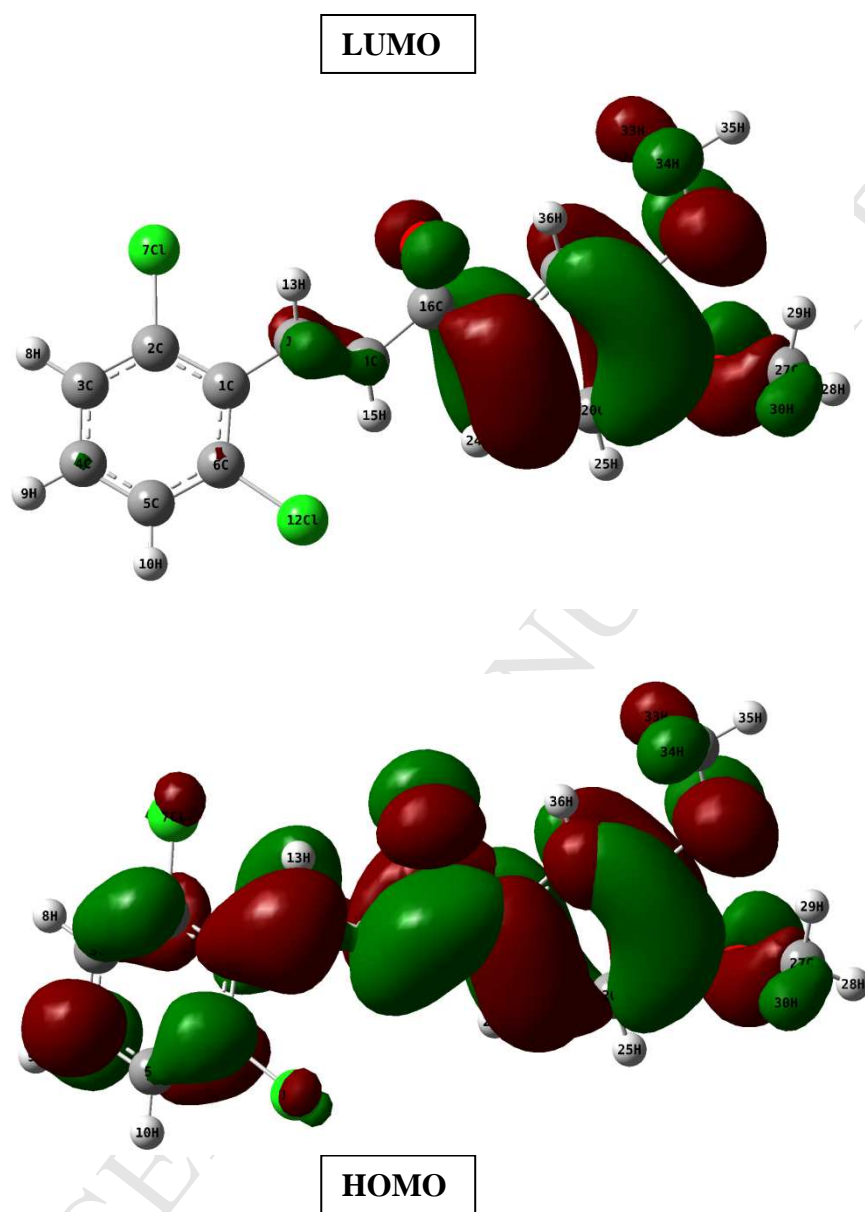


Fig. 5: Observed and calculated infrared spectrum of the compound



**Fig. 6:** Observed and calculated Raman spectrum of the compound



**Fig.7:** HOMO-LUMO plot of the title compound

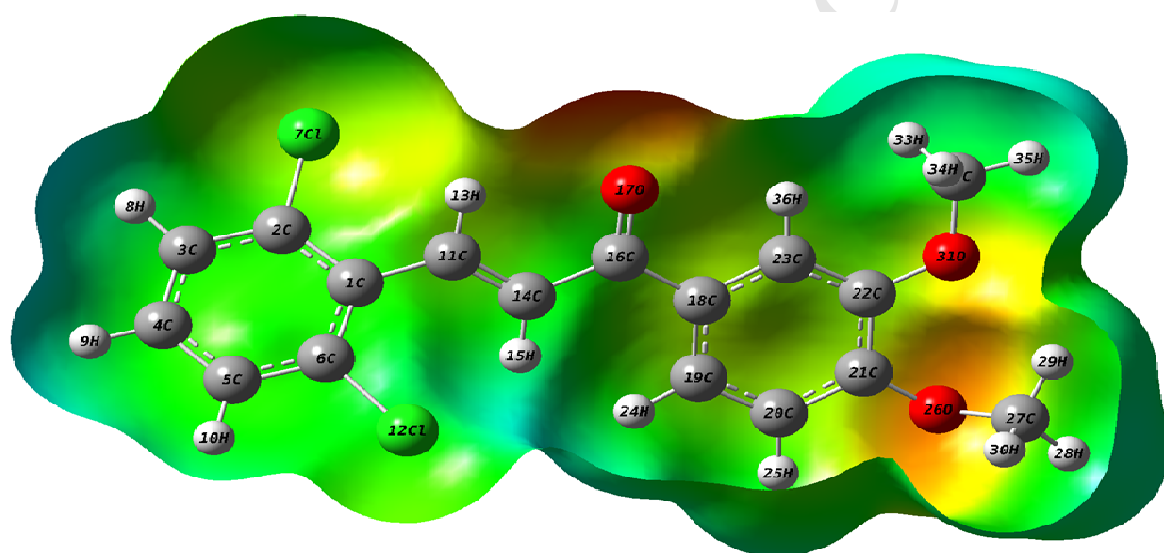


**Fig. 8:** The molecular electrostatic potential surface of the title compound

### Research Highlights

- ❖ 3D structure was confirmed by single crystal XRD data.
- ❖ The experimental results were supported by computational studies by using DFT.
- ❖ Theoretical calculations are in good agreement with the experimental results.
- ❖ The nonlinear optical properties and natural bond orbital analysis are theoretically predicted.